Tribology International 98 (2016) 144–154

Contents lists available at ScienceDirect

Tribology International

journal homepage: www.elsevier.com/locate/triboint

Rolling contact fatigue property and failure mechanism of carburized 30CrSiMoVM steel at elevated temperature

Guanghong Wang [a], Shengguan Qu [a,*], Lianmin Yin [a], Xiaoqiang Li [a], Wen Yue [b], ZhiQiang Fu [b]

[a] School of Mechanical and Automotive Engineering, South China University of Technology, Guangzhou 510640, China
[b] School of Engineering and Technology, China University of Geosciences (Beijing), Beijing 100083, China

ARTICLE INFO

Article history:
Received 18 December 2015
Received in revised form
26 January 2016
Accepted 23 February 2016
Available online 2 March 2016

Keywords:
Rolling contact fatigue
Carburized
Tribofilm
Failure mechanism

ABSTRACT

Rolling contact fatigue (RCF) behavior of carburized 30CrSiMoVM steel was experimentally investigated at elevated temperature. The results show that RCF crack was drive by asperity contact rather than the orthogonal shear stress or the maximum shear stress. The value of L_{10}, L_{50}, L_a life at 100 °C decreased by 48.3%, 44.1%, 43.2%, respectively, compared with that at 40 °C, which was attributed to lubrication status changing from mixed lubrication regime to boundary lubrication regime. The formation of the synergistic tribofilm containing Fe_2O_3, FeS, ZnS, $FePO_4$ and $Ca_3(PO4)_2$ around the center of the contact area effectively prevented initiation and propagation of RCF crack under boundary lubrication status, resulting in the obvious variation of the failure mode of the carburized layer.

1. Introduction

RCF is a typical failure mode in the mechanical products such as bearing, gear, wheel and rail pair, camshaft, etc. These parts are susceptible to fail due to suffering high speed, high cyclic stress, and high impact. Pitting, spalling, and delamination are often serious problems in industrial applications [1]. Generally, the RCF cracks initiate at the surface or subsurface. Therefore, RCF resistance can be improved by surface techniques such as thermal-spraying [2,3], plasma nitriding [1], carburization [4], shot peening [5,6], etc. Among them, carburization is a conventional and economic approach employed to enhance the RCF properties for steels because it can introduce a thick enough case as well as compressive residual stress.

The RCF resistance of the aforementioned key parts in transmission system is affected by many factors such as material microstructure and cleanliness, residual stress, heat treatment, geometry, service conditions, etc. Moghaddam et al. [7] investigated the influence of different inclusion characteristics such as size, depth, and stiffness on the RCF life of 8620 bearing steel. Shen et al. [8] revealed that the material with higher level of retained austenite and compressive residual stresses demonstrated higher RCF life. RCF performance of alumina ceramics thermally sprayed on steel roller was significantly affected by coating thickness [9]. It was reported that RCF life increased with the surface hardness of a carburized layer in Ref. [10]. However, RCF resistance is not only related with the surface hardness but also dependent on the substrate hardness [11]. Piao et al. [12] concluded that Fe–Cr coating with lower surface roughness had a higher RCF life. Zhang et al. [13] pointed out that load levels caused the failure mechanism change of the Ni-based alloy and WC–Ni ceramic composite coatings. Additionally, RCF life became more discrete and more difficult to predict as contact stress increased. Nejad et al. [14] studied effect of wear on rolling contact fatigue crack growth in rails. The results of their survey showed that high wear rate can lead to initial crack elimination and prevent their growth.

Most of the previous studies on the RCF performance of various materials have been completed at ambient temperature. However, some key parts such as camshaft in gasoline and diesel, bearing in aircraft gas-turbine engines sustain various high temperatures. Nevertheless, RCF behavior of the material at elevated temperature has not been reported yet. In addition, the decomposition of lubricating oil and the formation of tribofilm were demonstrated to have a significant influence of the tribological behavior of the sliding pairs [15,16]. However, the tribochemical reaction between the lubricating oil and the rolling elements has not been revealed yet. In this paper, rolling contact fatigue property of carburized 30CrSiMoVM steel at elevated temperature was investigated in comparison with that at the low temperature. Further, the effect of the tribofilm generated at the high temperature on the RCF failure mechanism was analyzed in detail.

* Corresponding author. Tel.: +86 20 87111983; fax: +86 20 87112111.
E-mail address: qusg@scut.edu.cn (S. Qu).

http://dx.doi.org/10.1016/j.triboint.2016.02.036
0301-679X/

2. Experimental details

2.1. Material preparation

The RCF samples with ring-type geometry used in this work were made of 30CrSiMoVM steel, which has a high strength and high impact toughness after hardening and tempering. The nominal composition is listed in Table 1. The thickness, external diameter and internal diameter were 4 mm, 60 mm and 30 mm, respectively. As shown in Fig. 1, the samples were firstly carburized at 920 °C for 6 h with a carbon potential of 1.3% in an IPSEN industrial RTQF–10–ERM furnace and then air cooled. The carburized samples were austenitized at 840 °C for 1 h and then oil quenched, followed by tempering at 180 °C for 3 h. After heat treatment, the samples were finally grinded and ultrasonically cleaned for 10 min in acetone for RCF tests.

2.2. Microstructure characterization and RCF tests

The cross-sectional hardness of the carburized layer was measured using a FM-300 microhardometer at the applied loads of 0.2 kg with the loading time of 10 s, obtaining the final result of every point from the average of five measurements. The surface microstructure of the carburized layer was observed using a Quanta 200 SEM. X-ray diffraction (XRD) analysis was conducted on a D8 ADVANCE diffractometer with Cu-Kα ($\lambda = 1.54056$ Å) excitation radiation to obtain the phase structure of the carburized surface. The scan angle (2θ) ranged from 30° to 90°. The surface profile and roughness of the samples were examined using a BMT 3D profile. X-ray photoelectron spectroscopy (XPS) analyses were carried out on a Thermo Fisher Scientific K-Alpha instrument equipped with an Al source (1486.8 eV). The C 1s peak at 284.8 eV was used as reference to correct the charging effect.

RCF tests were completed using a rolling contact fatigue test rig. The schematic of the machine is shown in Fig. 2. The specimen was fixed by three pins in the oil cup. The bearing with 11 uniformly distributed balls was employed as the counterpart. The balls were made of AISI52100 steel, with a diameter of 11.09 mm, an average surface roughness (R_a) of 0.025 μm, and a Rockwell C hardness of 60 HRC. The rotation velocity of the upper bearing was controlled by the spindle driving motor and it was kept to be 1600 ± 20 rpm. The normal force was loaded by a hydraulic cylinder. In order to make the force load uniformly upon each ball, a spherical contact was introduced. On this basis, the load of each ball was applied 750 N. A heating piece was fixed at the bottom of the oil cup. Air cooling system was normally open. Thus, the temperature equilibrium can be obtained by adjusting the heating and cooling systems. RCF tests were completed in two groups. One group was conducted at 40 °C and the other was performed at 100 °C. An acceleration transducer was fixed on the cylindrical surface of the oil cup to detect the vibration level to control the halting of the machine. The machine stopped automatically when the vibration level exceeded the preset value. Typical variations versus time of the acceleration signal at different temperatures are shown in Fig. 3. Both the temperature and acceleration curves only slightly fluctuated during the tests. When the samples failed the acceleration became bigger violently. All the tests were lubricated by Mobil Machine 0W-40CF Oil. The viscosity of the oil is 75 cSt at 40 °C and 13.5 cSt at 100 °C, with a density of 0.85 g/cm^3. Eight rolling contact tests were carried out to obtain the statistical result for each group.

3. Stress distribution

In this work, the contact stress distributions within the carburized layer were predicated using finite element model (FEM). The normal maximum stress at the contact center (P_o) and the contact radius (a) were calculated by Hertz's theory [17], and they were evaluated to be 4 GPa and 300 μm, respectively. For all calculation, pure rolling contact was only considered. That is, the friction coefficient between the ball and the sample was set to zero. Hence, the radius stress distribution at the contact surface can be determined by the equation [18],

$$P(r) = P_o\sqrt{1-\left(\frac{r}{a}\right)^2} \quad (0 \le r \le a) \tag{1}$$

where r is the distance from the contact center.

The FEM was created by using the commercial finite element analysis code ANSYS 14.0. The contact stress distribution $p(r)$ in Eq. (1) was applied on the contact surface as a pressure function, and the two-dimensional model is shown in Fig. 4. The distribution of radius stress (σ_r) on the carburized surface, the orthogonal shear stress (τ_{xy}) and the maximum shear stress (τ_{max}) along the thickness direction are shown in Fig. 5. The calculation of τ_{max} follows Tresca criterion. It is clear that the location of τ_{max} is generally deeper than that of the τ_{xy}. The depth of τ_{max} is about 220 μm, whereas the depth of the τ_{xy} is approximately 160 μm. For the σ_r, it is obvious that the contact area suffers compressive stress and the maximum radius stress locates at the contact center. In particular, σ_r changes from compression to tension around the contact edge and the maximum tensile stress appears at the edge, which may lead to crack initiation.

4. Results and discussion

4.1. Characterizations of the carburized layer and roughness

The cross-sectional morphology and microhardness distribution from the surface to interior of the carburized layer are shown in Fig. 6(a). It is clear that the hardness of the substrate is 520 $HV_{0.2}$. If the hardness of 570 $HV_{0.2}$ is considered as the threshold

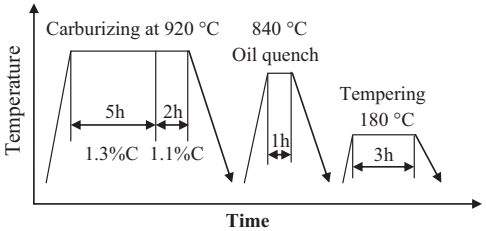

Fig. 1. Schematic diagram of the carburizing and heat–treatment process.

Table 1
Chemical compositions of the 30CrSiMoVM steel.

Material	Compositions (wt%)							
	C	Si	Mn	Cr	Mo	V	Nb	Fe
30CrSiMoVM	0.35	0.60	0.63	1.25	0.49	0.31	0.05	Balance